Lecture Notes in Mechanical Engineering

Rajana Suresh Kumar
Shubhashis Sanyal
P. M. Pathak *Editors*

Recent Advances in Machines, Mechanisms, Materials and Design

Select Proceedings of iNaCoMM 2023

Springer

Development of an Intelligent Image Recognition System for a Single Actuating Wave Robot

Natesan Sivaramakrishnan, N. Lokesh Kumar, S. Surya, V. Bevan, and A. R. R. Vijayaragavan

1 Introduction

Researchers have been analyzed the extensive use of legs for the locomotion of the robot. Over a decade ago, the researchers have started to analyze the locomotion of the robot crawling by utilizing the sine wave advancement. Researchers take inspiration from the nature, viz. limbless animals and biological systems, and also attempt to replace conventional locomotion patterns with alternate patterns. Gray [1] has illustrated the locomotion of the Tropidonotus natrix snake with the serpentine and crotaline motions. The author has also modeled the body of the snake as the series joining of the link to form the chains to achieve the motions. These links are modeled as elastic spring element to provide energy for the advancement of locomotion. Kane and David [2] have presented the detailed method of analysis of a stanford arm by using Kane's dynamical equation to show the improvements in the computational efficiency. The authors have framed the mathematical modeling of equation of motion of stanford arm by incorporating generalized speeds, generalized inertia forces, generalized active forces, partial velocities, and partial angular velocities. Shugen [3] has derived a serpentine curve under constant velocity conditions to analyze snake locomotion. The research investigated the ratio of tangential to normal force and locomotion power for efficiency. Computational results demonstrate improved agreement with existing experimental data compared to the clothoid spiral

N. Sivaramakrishnan (✉)
Tamil Nadu Centre of Excellence for Advanced Manufacturing, TANCAM, TIDCO, Chennai, Tamil Nadu 600113, India
e-mail: sivaramakrishnan@tancam.in

N. Lokesh Kumar · S. Surya · V. Bevan
Department of Mechanical Engineering, Saveetha Engineering College, Chennai, Tamil Nadu 602105, India

A. R. R. Vijayaragavan
Department of Artificial Intelligence and Data Science, Saveetha Engineering College, Chennai, Tamil Nadu 602105, India

R. S. Kumar et al. (eds.), *Recent Advances in Machines, Mechanisms, Materials and Design*, Lecture Notes in Mechanical Engineering,
https://doi.org/10.1007/978-981-97-5423-6_56

method. Pavel et al. [4] have used modern control theory, the authors examined snake body dynamics. They utilized the PD control with a Lyapunov function method to analyze the locomotion trace. Optimal parameters w and k were determined for the serpenoid curve across various link numbers. Yim et al. [5, 6] have developed Polybot, the first self-reconfiguring robot. They established two distinct snake locomotion modes, defining the robot with two modules: a segment with one DOF and two connection parts, and a node with no DOF and six connection parts. They created two robot systems, G1 and G2, for experimentation. G1, the first generation, consists of 32 modules controlled by limb movement patterns. G2 is an extension of G1, forming the second-generation system. Sato et al. [7] explored snake robot serpentine locomotion. Authors created a mathematical model for snake locomotion with n links and $n-1$ joints, considering directional frictional forces. They used simple and Coulomb friction models for analysis and evaluated serpentine limb locomotion from a power requirement perspective. Pei et al. [8] have developed the MERbot, a multi-dimensional elastomer robot for actuation and sensing. It comprises two types of spring rolling elements: 2 DOF and 3 DOF, which can self-align after two or four revolutions. The MERbot has six legs, each with 2 DOF. The authors used highly pre-strained 3M VHB 4910 acrylic adhesive films at 5–6 kV. The 2 DOF MERbot measures 1.4 cm in diameter, 6.8 cm in length, weighs 11 g, and can achieve a maximum bending angle of 90°. It can handle a maximum lateral force of 0.7 N and a blocked axial force of 15 N. The 3 DOF MERbot is 2.3 cm in diameter, 9 cm in length, weighs 29 g and can achieve a maximum bending angle of 35°. It can handle a maximum lateral force of 1 N. The authors connected the six spring rolls in series in two configurations, LRLRLR and RLRLRLR, and supplied 6 kV power to achieve serpentine locomotion. Li et al. [9] have analyzed the locomotion of the snake by incorporating the dynamic effect of friction between the link and the ground and derived the relation between input torque on the joint and driving forces with the body. The simulation has been carried out the calculate the torque acting on the joint by using the dynamic model of the locomotion of the snake. Alexander et al. [10] have designed a novel robot that uses continuous wave peristalsis for versatile crawling in confined spaces. This robot employs a braided mesh exterior technique to achieve smooth, worm-like locomotion. The robot's muscles expand and contract in both axial and circumferential directions, and the braided mesh exterior operates based on this principle of muscle expansion and contraction in both directions. Juhasz et al. [11] have simulated the locomotion of the worm. The authors have modeled the body of the worm as a MDOF system with the lumped mass. The model has artificial system-based actuator to provide the uniform motion to the system. Rezapour et al. [12] have examined path following control for a snake robot through virtual holonomic constraints. They derived the robot's equation of motion using the Lagrangian method, with the robot's geometry defined by these virtual holonomic constraints. Stabilizing the robot's constraints was achieved by implementing an input and output feedback linearizing control law. Luo et al. [13] have derived the dynamical modeling of pressure-operated snake robot with the basic requirements of optimization, sensing, control, and learning algorithms. A bending-type fluidic elastomers actuator has been used for the actuation of the robot. The theoretical results have been compared

with the existing experimental results of snake locomotion with the frictional characteristics. Zarrouk et al. [14, 15] have developed a very first robot which is driven by a single actuator. Zarrouk et al. [14] have used a single actuator with a worm gear. The rotary motions have been transmitted to the legs with the help of idler. There are six legs on each side of the robot. Each leg has a tripod. So that, it can be able to take right or left turn. Zarrouk et al. [15] developed a single actuating wave robot which can be able to actuate continuously in forward and backward motion. The advantage of the robot is that it does not have any spine link for the locomotion which is connected with a single DC motor. The authors have developed two different robots for the experimental verification. The authors have also demonstrated the design, kinematic modeling of the single actuating wave robot. Ariizumi et al. [16] have conferred with the kinematic calculation and a control method for the locomotion of the snake robot. The authors have modeled the kinematic motion in terms of semilinear partial differential equation. The authors have stated the attention required for the effect of singularities of links which are connected in series. Rafsanjani et al. [17] have incorporated the kirigami principle to increase the crawling capacity of a soft actuator. The authors have demonstrated the transformation of flat sheet to 3D-textured surfaces into scaled skin of a snake. This model helps in the reduction of direct frictional properties of the robot with the contacting surface which leads to further improvement in the crawling. Hosny et al. [18] underscore AI's potential to transform radiology, enhancing diagnostic accuracy, efficiency, and patient outcomes. AI algorithms excel in analyzing vast imaging datasets, supporting radiologists in detecting and characterizing diseases like cancers, cardiovascular conditions, and neurological disorders. These AI tools facilitate early detection, risk prediction, and personalized treatment planning. The authors delve into various AI techniques in radiology, including machine learning, deep learning, and natural language processing, showing their applications in computer-aided detection, image segmentation, and radiomics-based models for treatment response and prognosis prediction. Chandadevi et al. [19] offer a thorough examination of AI's applications in the fashion and apparel industry. It provides an in-depth analysis of various AI techniques used for trend forecasting, product design, virtual try-on, personalized recommendations, inventory management, and supply chain optimization. The authors also address the advantages and challenges of AI adoption, emphasizing improved efficiency, customer experience, and sustainability. This comprehensive review serves as a valuable resource for industry professionals and researchers, offering insights into the current state and future potential of AI in this sector. Guanhao et al. [20] offer a detailed overview of AI techniques in image recognition, covering deep learning, CNNs, and GANs. It explains their fundamental principles, architectures, and applications in object detection, facial recognition, and medical image analysis. The paper acknowledges challenges like data scarcity, computational complexity, and ethical concerns. While comprehensive, it would benefit from more empirical evidence and a deeper exploration of ethical implications. Zhiliang et al. [21] introduce a face mask recognition system based on the YOLOV5 algorithm for image recognition. It outlines an approach to detect and classify whether individuals wear face masks, explaining how they adapted the YOLOV5 model for this purpose. The study covers the

dataset, system implementation, and performance evaluation, which includes accuracy, precision, recall, and $F1$-score. The results indicate the system's effectiveness in detecting and recognizing face masks. The paper concludes by discussing practical applications and future developments, highlighting the YOLOV5 algorithm's potential for real-world deployment in various settings, contributing to image recognition. Huixian [22] delves into plant image recognition using deep learning and artificial neural networks (ANNs). The author explores their potential in accurately identifying plant species from images, emphasizing the use of convolutional neural networks (CNNs) for feature extraction and classification. Challenges like dataset preparation, model training, and evaluation metrics are addressed. Through experiments on a plant dataset, the author demonstrates that deep learning and ANNs achieve high accuracy in plant image recognition. The paper concludes by highlighting practical applications in agriculture, forestry, and environmental conservation. Overall, it advances plant image recognition by showcasing the capabilities of deep learning and ANNs, with implications for various industries and research fields. Numerous research papers have been published on topics such as locomotion of robots, single actuating wave robots, and deep learning methods for image recognition. However, there is a scarcity of literature that focuses specifically on the integration of image recognition systems into robots. Therefore, the present work is mainly focused on the following:

- The kinematic motion of the SAW robot has been studied and presented.
- Manufacturing of components of SAW such as helix, connecting rod, and links by using 3D printing fused deposition machine and developing the single actuating wave robot.
- Developing and incorporating an image recognition device on a single actuating wave robot.
- Testing of deep learning techniques for common dandelion and rose flowers.

2 Kinematic Modeling of Single Actuating Wave Robot

The analysis of traveling wave of the SAW robot and the comparison of traveling wave with the rotating helix and the kinematic analysis of the links have been presented in this section.

$$y = A \sin(\omega t), \tag{1}$$

where A is the amplitude of the wave and ω is the angular frequency.

Figure 1 shows a traveling sinusoidal wave. Suppose, the wave velocity is "v." If the disturbance takes time "t" to reach the point "P," then there will be different phases of wave at that point. So, displacement at that point becomes,

$$y = A \sin(\omega t - \phi). \tag{2}$$

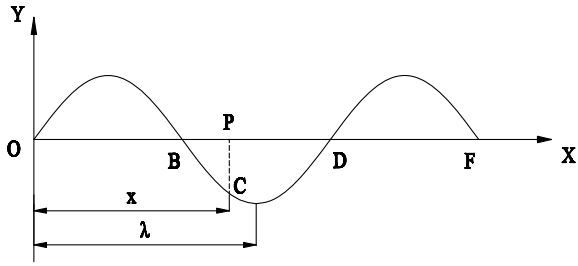

Fig. 1 A traveling sinusoidal wave

If "x" is corresponding path difference, so

$$\phi = \left\{\frac{2\pi}{\lambda}\right\} x. \tag{3}$$

2.1 Mathematical Model of Helix and Its Projection

A helical curve with its axis in the x-direction is given by the following parametric equations:

$$\begin{aligned} x &= \left(\frac{L}{2\pi}\right) c \\ y &= A\sin(c) \\ z &= A\cos(c), \end{aligned} \tag{4}$$

where L is the length of the pitch, A is the radius of helix, c is the unconstrained parameter. We know from equation of helix

$$\begin{aligned} x(t) &= ht \\ y(t) &= R\sin(t) \\ z(t) &= R\cos(t) \end{aligned} \tag{5}$$

By using Eqs. 4 and 5, the unconstrained parameter c can be determined.

$$\begin{aligned} t = c &= \left(\frac{2\pi}{L}\right) x \\ h &= \left(\frac{L}{2\pi}\right). \end{aligned} \tag{6}$$

In 2D,

$$\begin{aligned} x &= \left(\frac{L}{2\pi}\right) c \\ y &= A\sin(c) = A\sin\left(\frac{2\pi x}{L}\right). \end{aligned} \tag{7}$$

2.2 Equation of Rotating Helix and Comparison to Transverse Wave

To perform rotation using a rotation matrix R; the position of each point must be represented by a column vector V. So,

$$V_1 = RV.$$

In 3D, the basic rotation matrices by an angle θ about x-, y-, and z-axes are given by

$$R_x(\theta) = \begin{bmatrix} 1 & 0 & 0 \\ 0 & \cos(\theta) & -\sin(\theta) \\ 0 & \sin(\theta) & \cos(\theta) \end{bmatrix} \tag{8}$$

$$R_y(\theta) = \begin{bmatrix} \cos(\theta) & 0 & \sin(\theta) \\ 0 & 1 & 0 \\ -\sin(\theta) & 0 & \cos(\theta) \end{bmatrix} \tag{9}$$

$$R_z(\theta) = \begin{bmatrix} \cos(\theta) & -\sin(\theta) & 0 \\ \sin(\theta) & \cos(\theta) & 0 \\ 0 & 0 & 1 \end{bmatrix} \tag{10}$$

However, the helix is rotated about x-axis at a constant angular frequency ω. The parametric equation of helix is multiplied by the rotation about x-axis.

$$\begin{bmatrix} x(c,t) \\ y(c,t) \\ z(c,t) \end{bmatrix} = \begin{bmatrix} 1 & 0 & 0 \\ 0 & \cos(\omega t) & -\sin(\omega t) \\ 0 & \sin(\omega t) & \cos(\omega t) \end{bmatrix} \begin{bmatrix} \frac{Lc}{2\pi} \\ A\sin(c) \\ A\cos(c) \end{bmatrix} = \begin{bmatrix} \frac{Lc}{2\pi} \\ A\sin(c-\omega t) \\ A\cos(c-\omega t) \end{bmatrix} \tag{11}$$

Figure 2 shows the projection of a 3D helix wave and its projection on $X-Y$ and $X-Z$ plane.

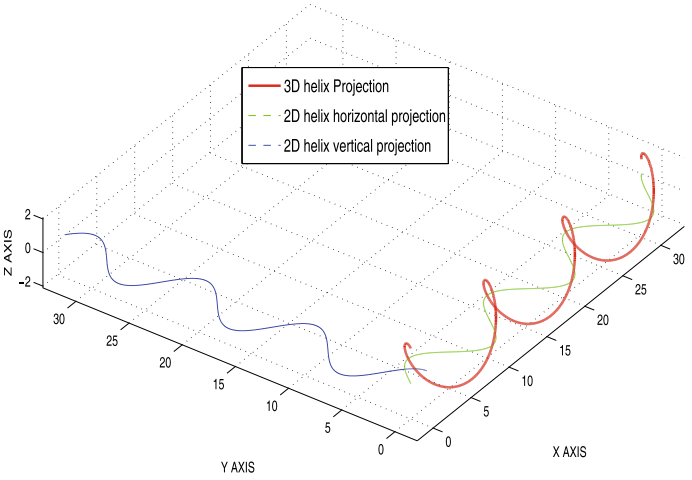

Fig. 2 A helix and its projection on X–Y and X–Z plane

2.3 *Kinematics of the Links*

The kinematics of the links is being analyzed and a relation is being set up with the velocity of the wave and the velocity of the link. If f is the frequency of locomotion, L_{wave} is the wavelength, A is the amplitude of the wave, L_{cycle} is the net advance per cycle(one rotation of the helix).

Then the advance ratio (AR) is defined as the ratio of speed of the robot (V_{robot}) and the speed of the traveling wave relative to the motor base (V_{wave}).

$$AR = \frac{V_{\text{robot}}}{V_{\text{wave}}} = \frac{L_{\text{cycle}}}{L_{\text{wave}}} \tag{12}$$

$$V_{\text{robot}} = f L_{\text{cycle}} \tag{13}$$

During the motion of the robot, the links move both horizontally and vertically. As the wave advances by Δx, the link will rotate by $\Delta\beta$.

Therefore,

$$\Delta\beta \underset{(x=\Delta x)}{=} a\tan\left(\frac{\mathrm{d}}{\mathrm{d}x}(A\cos(kx))\right) \tag{14}$$

$$= a\tan(-kA\sin(k\Delta x))$$

Then the tip of the link will move horizontally by a distance ΔX:

$$\Delta X = r\sin(\Delta\beta) \tag{15}$$

If the speed of the wave is V_{wave}, the time required by the wave to advance by a distance of Δx is given by:

$$\Delta t = \frac{\Delta x}{V_{\text{wave}}}. \tag{16}$$

Therefore, the expected speed of the links is:

$$V_{\text{link}} = \frac{\Delta X}{\Delta t}. \tag{17}$$

Inserting Eqs. 14 to 16 into 17, the speed of the tip of the link is obtained as:

$$V_{\text{link}} = \frac{r \sin(a \tan(-kA \sin(k\Delta x)))V_{\text{wave}}}{\Delta x}. \tag{18}$$

Assuming $\Delta\alpha$ to be very very small,

$$\Delta\beta \ll 1 \Rightarrow \begin{cases} \sin(k\Delta x) \approx k\Delta x \\ a \tan(Ak^2\Delta x) \approx Ak^2\Delta x \end{cases} \tag{19}$$

Putting Eq. 19 into 18, the speed of the tips of the links as a function of the height r, amplitude A, wavelength L_{wave}, and wave speed V_{wave}

$$V_{\text{link}} \approx rAk^2V_{\text{wave}} = rA\left(\frac{2\pi}{L_{\text{wave}}}\right)^2 V_{\text{wave}} \tag{20}$$

The speed of the wave can also be calculated as a function of the actuation frequency:

$$V_{\text{link}} \approx rAk^2V_{\text{wave}} = (2\pi)^2\frac{A}{L_{\text{wave}}}rf \tag{21}$$

It has been noticed that speed of the link is proportional to the ratio of amplitude and the wavelength multiplied with the height of the links and with the actuation frequency which is shown in Eq. 20. Figure 3 shows the rotations of the link.

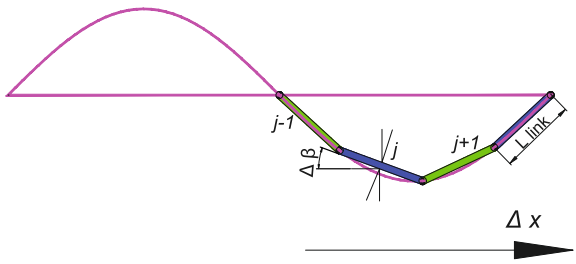

Fig. 3 Rotation of the link

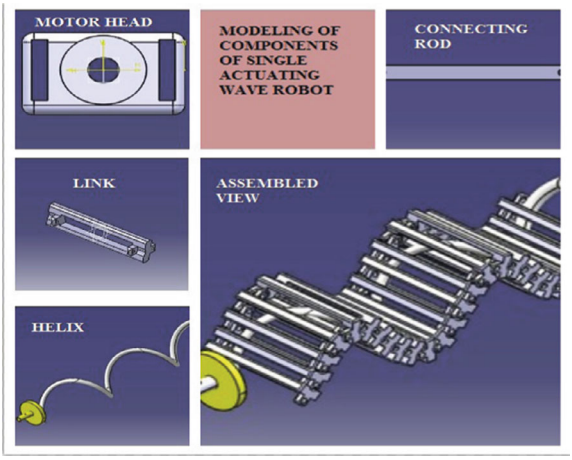

Fig. 4 Components of SAW robot

3 Development of SAW Robot by Using 3D Printing Technology

The components of a single actuating wave robot, including the helix, link, connecting rod, and motor head, were designed using CATIAV5. Figure 4 displays these robot components. They were 3D printed using an FDM 3D printer, as shown in Fig. 5. Polylactic acid (PLA) is a common thermoplastic polyester made from fermented plant starch, often using corn starch as the raw material. It's widely used in 3D printing due to its various properties, listed in the table. Unlike plastics like ABS or polycarbonate, PLA is primarily intended for 3D printing. It's available in a variety of colors and is compatible with most 3D printers, not requiring a heated bed and using lower printing temperatures. Figure 6 depicts the SAW robot.

4 Implementation of ESP32 Camera Module and FTDI Adapter for Live Tracking

ESP32 Camera Module by Espressif Systems is a very powerful module with built-in Wi-Fi and Bluetooth SoC and a 2 Megapixel camera. This camera module can be coded with Arduino IDE using the example code available for AI Thinker Camera. To upload code on the board an FTDI adapter is used, which provides connectivity to a computer since ESP32 Module cannot be directly connected to a computer. FT232R driver is needed to be installed in the computer first in order to use the FTDI Adapter. This module can be powered by either $3.3V_{dc}$ or $5V_{dc}$. After uploading code into the board, with the IP Address provided by the system the camera can be accessed remotely within range. This module provides the facility to capture figures or even

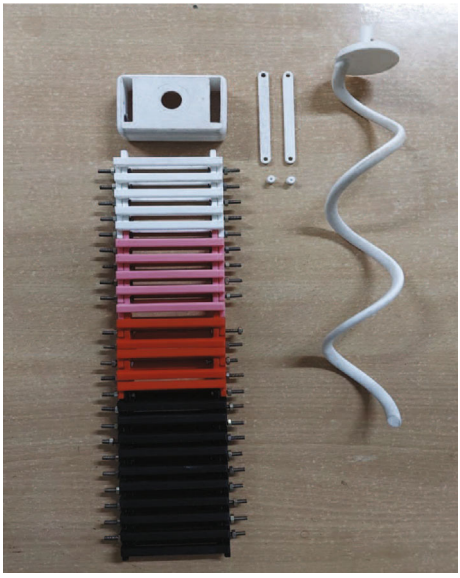

Fig. 5 3D-printed components of SAW

Fig. 6 Single actuating wave robot

take a video with different resolution options. This module also has a dedicated microSD card slot that can be used to store the figures. The specifications of ESP32 module are main processor: Tensilica Xtensa 32-bit LX6 microprocessor, Cores: 2 or 1 (depending on variation), Clock frequency: up to 240 MHz, Performance: up to 600 DMIPS; Wireless connectivity:Wi-Fi: 802.11 b/g/n/e/i (802.11n @ 2.4 GHz up to 150 Mbit/s), Bluetooth: v4.2 BR/EDR and Bluetooth Low Energy (BLE); Internal memory: ROM: 448 KiB, SRAM: 520 KiB, RTC fast SRAM: 8 KiB, RTC slow SRAM: 8 KiB, eFuse: 1 Kilo bit. Figure 7 shows the SAW robot with the implementation of ESP32 Camera Module and FTDI Adapter for Live Tracking. Figure 8 shows the image of testing of live tracking.

Fig. 7 Implementation of ESP32 camera module and FTDI adapter for live tracking

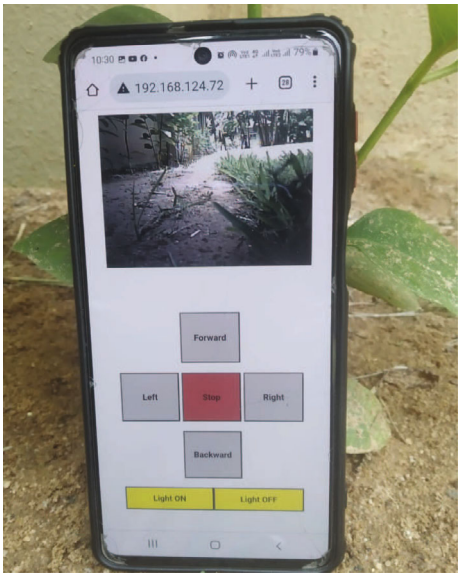

Fig. 8 Live tracking using SAW robot

5 Incorporation of ESP32 CAM to Capture the Image for Image Recognition

To set up the ESP32CAM, connect it to the FTDI adapter with jumper wires, ensuring proper pin connections for power, ground, TX, and RX. If you need to charge the ESP32CAM, use a booster circuit to stabilize and boost the input voltage for a reliable power supply, especially when input voltage is low. Design this circuit with suitable voltage regulators and capacitors to meet power requirements for the ESP32CAM and any attached components. The process is simple: update Wi-Fi credentials in the code, click Upload, observe connecting dots, press the RST button to start the

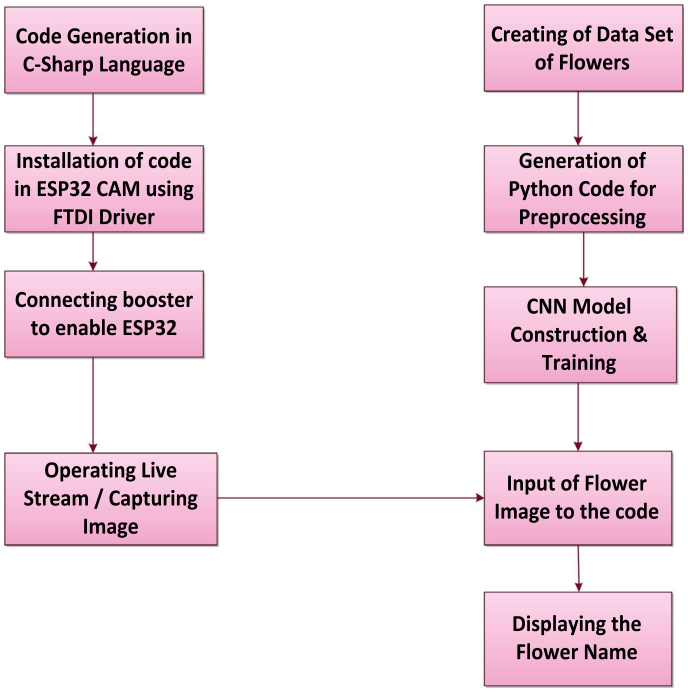

Fig. 9 Flowchart

upload, and when it's done, remove the GPIO1-GND jumper. Set the serial monitor to 115200 baud, press the RST button, and it will display the webserver's IP address for accessing ESP32CAM features like the camera.

6 Testing for Image Recognition

Figure 9 depicts the image recognition process for a flower. It begins by powering on the ESP32 CAM module, situated on the single actuating wave robot, functioning as the camera. The ESP32 CAM captures an image, saves it to internal storage, and retrievs its path. This path contains information for code input. The code reads the image, compares it to a flower dataset, and predicts the species. Outputs include the identified flower's name, an image for visual confirmation, and its classification category. In summary, the process involves powering up ESP32 CAM, image capture, path retrieval, code input, comparison to a flower dataset, species prediction, and display of relevant information.

Fig. 10 Process of robot taking an image of a flower

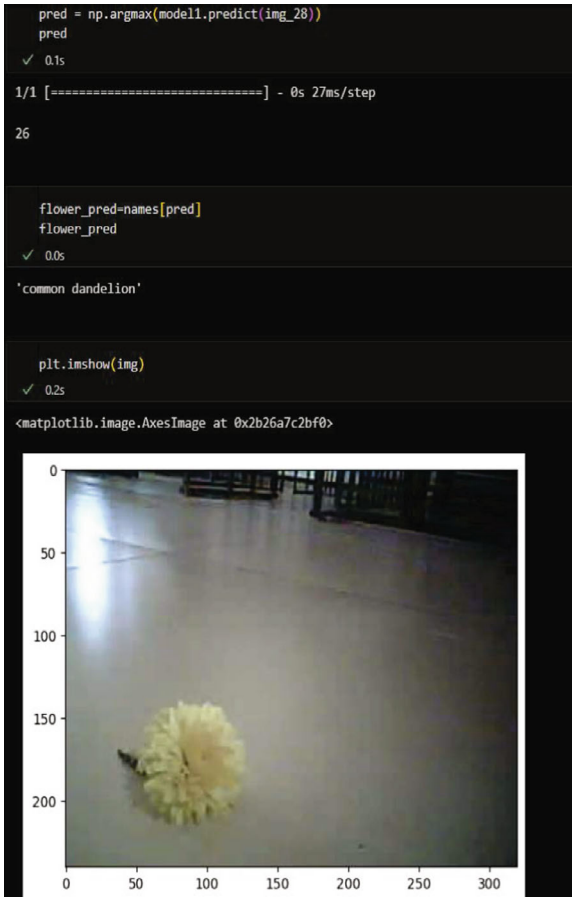

Fig. 11 Image recognition of a common dandelion flower

Figure 10 shows the SAW robot capturing an image of a "common dandelion" flower, while Figs. 11 and 12 display the results of image recognition for "common dandelion" and "rose" flowers, respectively.

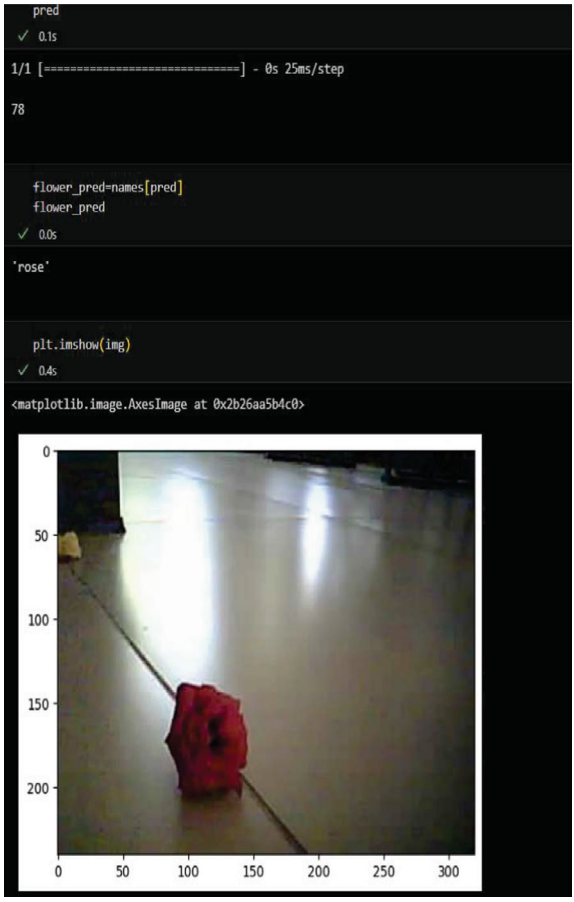

Fig. 12 Image recognition of a rose flower

7 Conclusions

In conclusion, this study successfully demonstrates the development and implementation of an intelligent image recognition system for a single actuating wave (SAW) robot using deep learning techniques. The research is divided into two main sections: creating the SAW robot and integrating the deep learning process for image recognition.

The SAW robot's motion harnesses the advancements in sine wave technology, and its kinematic motion is thoroughly examined and presented. The components of the SAW robot are fabricated through 3D printing using fused deposition, contributing to its overall efficiency and versatility.

The image recognition aspect of the project is of significant importance, as it enables the identification of objects stored within the device. By utilizing the ESP32 CAM, FTDI adapter, and a booster, the system captures images for subsequent recognition, allowing the robot to perceive and interact with its surroundings intelligently.

Python code is effectively employed to achieve image recognition, showcasing the feasibility and applicability of deep learning techniques in computer vision tasks. The obtained results demonstrate the system's ability to accurately identify objects, locations, individuals, and actions within images.

The developed SAW robot, equipped with the intelligent image recognition system, shows promising potential for live tracking applications. It has undergone thorough testing, affirming its capabilities and reliability in real-world scenarios.

Overall, this study lays the groundwork for further advancements in intelligent robotics, image processing, and computer vision, offering valuable insights and contributions to the field of automation and artificial intelligence. The developed system's successful integration of deep learning techniques paves the way for future research and applications in various industries, ranging from manufacturing and surveillance to healthcare and beyond.

References

1. Gray J (1946) The mechanism of locomotion in snakes. J Exp Biol 23:101–120. https://doi.org/10.1242/jeb.23.2.101
2. Kane T, Levinsion D (1983) The use of Kane's dynamical equations in robotics. J Mol Biol 2:3–21
3. Shugen MA (1999) Analysis of snake movement forms for realization of snake-like robots. In: IEEE international conference on robotics and automation, vol 4, pp 3007–3013. https://doi.org/10.1109/ROBOT.1999.774054
4. Pavel P, Mita T (1999) Control and analysis of the gait of snake robots. In: IEEE international conference on robotics and automation, vol 1, pp 502–507. https://doi.org/10.1109/CCA.1999.806692
5. Yim M, Duff D, Roufas K (2000) Polybot: a modular reconfigurable robot. In: Proceedings 2000 ICRA. Millennium conference. IEEE international conference on robotics and automation. Symposia proceedings (Cat. No.00CH37065), vol 1, pp 514–520. https://doi.org/10.1109/ROBOT.2000.844106
6. Yim M, Roufas K, Duff D, Zhang Y, Eldershaw C, Homans S (2003) Modular reconfigurable robots in space applications. Robotics 14:225–237. https://doi.org/10.1023/A:1022287820808
7. Sato M, Fukaya M, Iwasaki T (2002) Serpentine locomotion with robotic snakes. IEEE Control Syst Mag 22:64–81. https://doi.org/10.1109/37.980248
8. Pei Q, Rosenthal M, Stanford S, Prahlad H, Pelrine R (2004) Multiple-degrees-of-freedom electroelastomer roll actuators. Smart Mater Struct 13:86–94. https://doi.org/10.1088/0964-1726/13/5/N03
9. Li C, Shugen M, Wang Y, Li B, Duana D (2005) Design and modelling of a snake robot in traveling wave locomotion. Mech Mach Theory 42:1632–1642. https://doi.org/10.1016/j.mechmachtheory.2006.12.003
10. Alexander SB, Shaw KM, Chiel HJ, Quinn RD (2012) Continuous wave peristaltic motion in a robot. Int J Robot Res 31:302–318. https://doi.org/10.1177/0278364911432486
11. Juhasz Z, Zelei A (2013) Analysis of worm-like locomotion. Periodica Mech Eng 57:59–64. https://doi.org/10.3311/PPme.7047
12. Rezapour E, Pettersen KY, Liljebäck P, Gravdahl JT, Kelasidi E (2014) Path following control of planar snake robots using virtual holonomic constraints: theory and experiments. Robot Biomimetics 1:1–15 (2014). https://doi.org/10.1186/s40638-014-0003-6
13. Luo M, Agheli M, Onal C (2014) Theoretical modeling of a pressure-operated soft snake robot. In: Proceedings of the ASME 2014. International design engineering technical conferences

and computers and information in engineering conference, pp 1–9. https://doi.org/10.1115/DETC2014-35340
14. Zarrouk D, Fearing RS (2015) Controlled in-plane locomotion of a hexapod using a single actuator. IEEE Trans Robot 31:157–167. https://doi.org/10.1109/TRO.2014.2382981
15. Zarrouk D, Mann M, Degani N, Yehuda T, Jarbi N, Hess A (2016) Single actuator wave-like robot (SAW): design, modeling, and experiments. J Bioinspiration Biomimetics 11:1–13. https://doi.org/10.1088/1748-3190/11/4/046004
16. Ariizumi R, Tanaka M, Matsuno F (2016) Analysis and heading control of continuum planar snake robot based on kinematics and a general solution thereof. Adv Robot 30:301–314. https://doi.org/10.1080/01691864.2015.1118409
17. Rafsanjani A, Zhang Y, Liu B, Rubinstein SM, Bertoldi K (2018) Kirigami skins make a simple soft actuator crawl. Sci Robot 3:1–7. https://doi.org/10.1126/scirobotics.aar75
18. Hosny A, Chintan P, John Q, Lawrence HS, Aerts HJWL (2018) Artificial intelligence in radiology, vol 18. Macmillan Publishers Limited, part of Springer Nature, pp 500–510 (2018). https://doi.org/10.1038/s41568-018-0016-5
19. Chandadevi G, Sheenam J, Xianyi Z, Pascal B (2019) A detailed review of artificial intelligence applied in the fashion and apparel industry. IEEE Access 7:95376–95396. https://doi.org/10.1109/ACCESS.2019.2928979
20. Guanhao Y, Wei F, Jintao J, Lei Q, Li X, Gui G, Weijun W (2020) Face mask recognition system with YOLOV5 based on image recognition. In: 2020 IEEE 6th international conference on computer and communications (ICCC), pp 1398–1404. https://doi.org/10.1109/ICCC51575.2020.9345042
21. Zhiliang Z, Limei Z, Tao Y (2021) Research on the application of artificial intelligence in image recognition technology. J Phys Conf Ser 1992:1–4. https://doi.org/10.1088/1742-6596/1992/3/032118
22. Huixian J (2020) The analysis of plants image recognition based on deep learning and artificial neural network. IEEE Access 8:68828–68841. https://doi.org/10.1109/ACCESS.2020.2986946